International Journal of Heat and Technology
Vol. 36, No. 3, September, 2018, pp. 877-882
Journal homepage: http://iieta.org/Journals/IJHT

Fibre Bragg Grating sensing based temperature monitoring system of power transformer

Wei Wei, Hongzheng Mei, Peng Xue*

Changchun University of Technology, Changchun 130012, China

Corresponding Author Email: weiwei@mail.ccut.edu.cn

https://doi.org/10.18280/ijht.360314

Received: 17 January 2018
Accepted: 25 May 2018

Keywords:
Fibre Bragg Grating sensor, power transformer, monitoring system, GaAs material

ABSTRACT

In an electric power system, the upgrading of the power transformer level and capacity leads to the increase of failure rate and repair time. As a result, the transformer winding temperature is monitored in real-time to give early warning so that effective measures can be carried out to reduce the occurrence of incidents. The internal environment of a transformer is characterized by high voltage, strong electromagnetic interference, narrow space, and strong corrosion, etc. How to detect the transformer state in a stable, accurate and quick manner and precisely predict failures has become the critical technical difficulty requiring urgent solution. Therefore, researchers have been working on the application of sensing technologies in the health monitoring of large-sized equipment. The Fiber Bragg Grating (FBG) sensing technology is a rising interdisciplinary high-tech application. Compared with traditional sensors, a FBG sensor has such advantages as small volume, light weight, implantable structure, no electromagnetic interference and reusability, making it one of the core sensing elements widely applied in the field of equipment health monitoring. Being suitable for long-term monitoring in a severe environment, it is now a great substitute for electric sensors.

1. INTRODUCTION

A power transformer is the most important and expensive component in a power transmission and transformation network. Its reliable operation directly decides the safety and stability of the whole network. Most transformers come to the end of their service lives due to loss of insulation, which is mainly the result of the high temperature in the hottest zone of transformer winding in operation. The hot-spot temperature of transformer winding is not only the most important limiting factor to the load capacity of a transformer, but also related to its safety, reliability, service life and cost [1-3]. Therefore, accurate calculation and prediction of the transformer winding hot-spot temperature is very important to reasonably utilizing the maximum load capacity and extending the service lives of transformers. At present, winding temperature is usually simulated based on the top oil temperature and load current to provide some reference for the operation conditions of transformer. However, this method cannot give accurate, timely and visible results. Therefore, it is necessary to apply new technologies to realize real-time monitoring on the transformer winding temperature. The fiber online monitoring system for transformer winding temperature solves this problem perfectly. FBG temperature measurement is a convenient, accurate, safe and reliable technology to monitor transformer winding hot-spot temperature. It defects hidden risks such as winding over-temperature in a timely and accurate manner, which is of significance to the safe and reliable operation of transformers.

The heat dissipation in the winding of a transformer has great impacts on the working performance and reliability of the transformer. When the winding temperature rises to a certain limit, it will accelerate the aging of the insulation, or even damage the insulation, directly affecting the service life of the transformer. Therefore, it is necessary to calculate and predict the temperature distribution on the transformer winding under given conditions, using the electromagnetic field theory and the heat transfer theory, so as to obtain the thermal characteristics of the transformer. In this way, appropriate measures can be taken to increase the cooling effect of the transformer to ensure its safe operation. The heat generated by the transformer during operation is caused by all types of losses, so it is also very important to study how these losses occur. As a matter of fact, it is the precondition for studying the temperature field of the transformer. Only when the losses are well understood and can be accurately calculated, will the study on the temperature field be meaningful [4].

2. OVERALL DESIGN OF THE FBG TEMPERATURE MONITORING SYSTEM

The overall design of the FBG temperature measurement platform is shown in Fig. 1. The light emitted by the broad-band source is transmitted to the FBG sensor channel and the reference FBG channel respectively through a 2×2 fibre coupler. The FBG sensor channel is connected to multiple FBG sensors with non-overlapping centre wavelengths, and the reference FBG channel accommodates two reference FBGs, which are put into the environment with constant temperature and centre wavelength as reference. The band width of the FBG reflected light is about 0.2nm, the spectral width of the filter about 0.05nm, the centre wavelength 1550nm, and the free spectral range 40nm. The piezoelectrics (PZT) on the filter are controlled by the saw tooth wave to scan the free spectral range repeatedly [5-7]. When the wavelength of the filter coincides with the centre wavelength of the FBG sensor, the electrophotonic detector will detect the light

reflected by the FBG sensor. The voltage values in the electrophotonic detector are collected by a data acquisition card, and then input into a computer for processing. The FBG wavelength and temperature are obtained by calibration calculation.

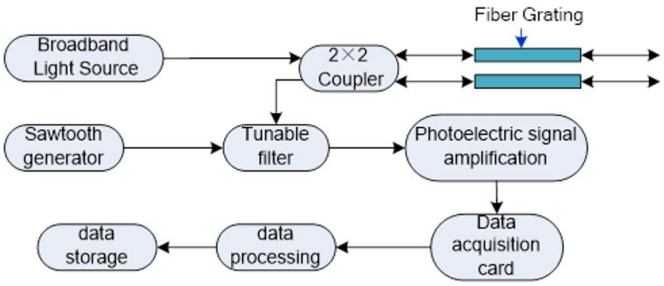

Figure 1. Diagram of the fibre grating temperature measuring system

The principle of fibre Bragg grating temperature measurement of transformer windings is briefly described as follows: the broadband light source is reflected by the Bragg grating as narrowband light, with its reflection wavelength depending on the grating period. When the external temperature changes act on the grating, the period and the effective refractive index of the fibre grating will vary, which will make the reflection wavelength change accordingly. The demodulation device converts the sensing signal of the wavelength code into a digital signal and sends it into the computer for real-time monitoring and processing.

Both temperature and stress changes can result in the wavelength drift of the fibre Bragg grating. When the electromagnetic wire of the embedded fibre Bragg grating sensor is being fabricated, the external temperature remains almost unchanged [8], so the wavelength changes of the fibre Bragg grating are mainly caused by the stress changes; in other words, by monitoring the wavelength variation of the optical fibre Bragg grating, we are able to obtain the stress state of the fibre Bragg grating sensor throughout the process. Based on the real-time monitoring data of the fabrication process, people can evaluate the impacts of stress fluctuations on the temperature characteristics and mechanical performance of the embedded FBG sensors and give suggestions on improving the manufacturing process of electromagnetic wires. In addition, the monitoring data can also provide reference for temperature compensation, stress desensitization and calibration of transduction factors.

3. SELECTION OF SYSTEM COMPONENTS

3.1 System light source and characteristics analysis

The conductor temperature sensing principle and characteristic analysis given above show that, the system light source should meet the following conditions:

(1) The spectrum on the right side of the light source covers the absorption wavelength range of the GaAs material (800nm~1000nm), and the spectral intensity on this side is in a linear relationship with the wavelength.

(2) The light source has high and stable output power.

(3) The light source is small with high luminous efficiency and long life, and convenient for installation. Considering the above conditions as well as the price, the high-performance toothed crane lamp with a peak wavelength of 800nm and a half-spectral width of 200nm is adopted in the system as a broadband light source, characterized by small volume, high power, small luminous attenuation, stable output, low price and long life. This halogen tungsten lamp has a MTTF of 11 years working with 100% design power; and when it works with 30% of the maximum load power, it will have a service life of 15 years or more. [9-10].

Considering the loss and viscosity of the oil with temperature changes, the Levenberg-Marquardt method is adopted in the top oil temperature rise test to determine the parameters of the improved model for the winding hotspot temperature based on the calculation results and the actual operation of the transformer. It is found out that the winding hotspot temperature of the oil immersed power transformer obtained in the laboratory is in good agreement with the actual monitoring results, with the errors being completely within the allowed range, which means this model can correctly reflect the hotspot temperature changes over time, and has good continuity. This improved model for winding hotspot temperature established in this paper can be used not only to calculate the winding hotspot temperature rises under various loads, but also to accurately obtain the actual operation status of the power transformer and its dynamic thermal behaviours. Jt meets the winding temperature monitoring requirements for large oil immersed power transformers [11].

Table 1. Comparison of characteristic variables for fault diagnosis

Transformer component	Temperature rise limit / ℃
Oil temperature rise at the top layer when oil is not in direct contact with the atmosphere	55
Oil temperature rise at the top layer when oil is in direct contact with the atmosphere	58
Average winding temperature rise	65
Mailbox surface	80

3.2 Basic composition of the sensing probe

A GaAs probe is the sensitive element of a sensing system, and its design is the core of temperature sensing, as it directly affects the system response time, temperature measuring range and precision, etc.

On the basis of the traditional structure, a novel reflective sensing probe is designed in combination with the modern GaAs film preparation technology. Fig. 2 shows the basic composition of the probe. The GaAs crystal in the probe, with a thickness of 110μm, is coated by a transmission film and a reflecting film, with good optical characteristics on the front and back sides. Then the GaAs crystal is fitted into a heat-resistant Teflon sleeve and fastened by evenly high-temperature adhesive, making the multimode optical fibre vertically coupled with the GaAs crystal to the maximum extent [11]. Having such advantages as corrosion and high temperature resistance and good insulation and heat conduction, etc., the Teflon sleeve is used for the purposes of fixation, heat conduction and electric insulation. The novel reflective sensing probe is small in volume and simple in structure, which is convenient for installation. The thin GaAs crystal and high coupling efficiency reduces the light attenuation and improves the measurement precision and response time of the system.

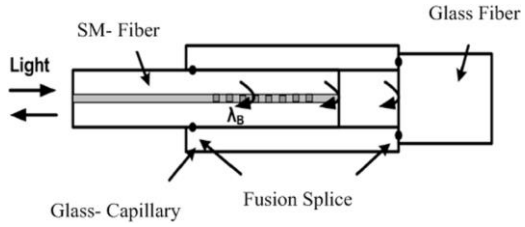

Figure 2. Material structure of an optical fibre sensor

3.3 Analysis of the optical fibre coupling with GaAs slice

The coupling design of the optical fibre and the GaAs slice is the key to fabricating a sensing probe. the higher coupling efficiency is, the smaller the light intensity loss will be and the stronger the effective light signal received will be. It also reduces other interferences from random coupling.

In the connection between the optical fibre and the GaAs slice, the luminous power transmitted in the optical fibre should be passed to the GaAs slice as much as possible to obtain the optimal coupling efficiency, and the light absorbed by the GaAs material should also be reflected to the demodulating system through the optical fibre as much as possible. This is a matter of the coupling between the optical fibre and the GaAs material.

In Fig. 3, there are many factors affecting the coupling efficiency of the optical fibre and the GaAs material, such as locations of the optical fibre and the GaAs material, selection of the transmission film and the reflecting film and quality of the GaAs material, etc. Based on the above analysis, the following measures are carried out in design to improve the coupling efficiency [12-14]:

(1) The GaAs slice is kept vertically fastened with the end face of the optical fibre to minimize the loss of the absorbed luminous power in the optical fibre.

(2) Multimode optical fibre is adopted to receive the light energy reflected to the maximum extent after the absorption by the GaAs material to improve the coupling efficiency.

(3) The GaAs material selected is of high purity and its end face is kept as smooth as possible.

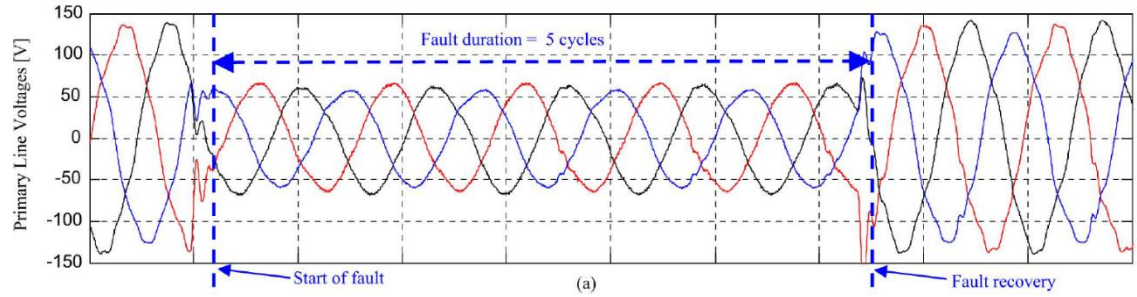

(a) Voltage simulation for optical power loss

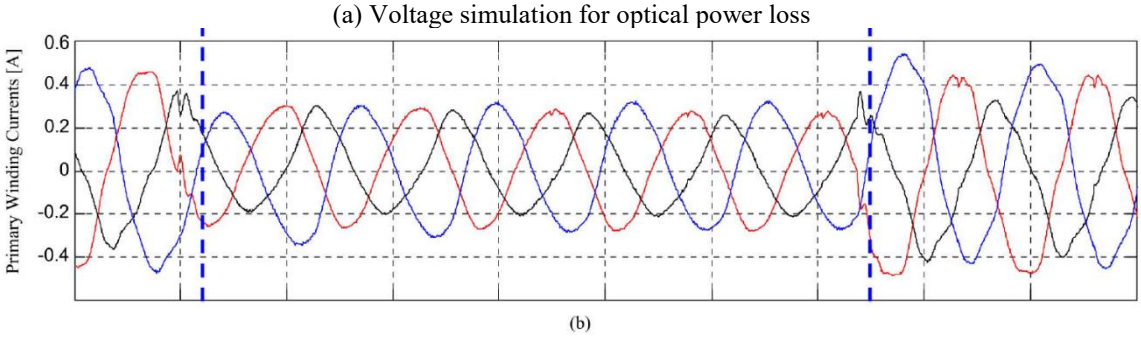

(b) Coupling efficiency simulation analysis

Figure 3. Simulation analysis on the coupling efficiency of the optical fibre and the GaAs slice

4. PERFORMANCE TESTING OF THE FBG TEMPERATURE MONITORING SYSTEM

4.1 Basic error test

The test procedures are as follows: insert the FBG temperature sensor to be tested and the thermocouple thermometer into the thermostatic bath. Maintain the temperature of the thermostatic bath at the specified temperature for the testing point, and read the normal thermometer. Then, read the tested temperature sensor. The difference between the temperature readings of the two is the basic error at this testing point. Part of the energy loss is distributed to the surrounding media. Some makes the transformer temperature increase, which can be expressed as follows according to the energy conservation law:

$$P_{ue0}dt = C_{ue0}d\Delta T + P_{ue0}\Delta T dt \tag{1}$$

Winding, core and transformer oil are the major components of an oil-immersed power transformer. These three parts are studied separately from the transformer for their temperature rise features and heating and cooling processes:

$$C_{ue1}d\Delta T_1 + (\Delta T_1 - \Delta T_3)P_{ue1}dt = P_{ue1}dt \tag{2}$$

$$C_{ue2}d\Delta T_2 + (\Delta T_2 - \Delta T_3)P_{ue2}dt = P_{ue2}dt \tag{3}$$

$$C_{ue2}d\Delta T_2 + \Delta T_3 P_{ue3} = (\Delta T_1 - \Delta T_3)P_{ue1}dt + (\Delta T_2 - \Delta T_3)P_{ue2}dt \tag{4}$$

Where, C_{ue1}, C_{ue2} and C_{ue3} are respectively the heat capacities of the winding, the core, and the transformer oil;

ΔT's are the temperature rises in the winding, the core and the transformer oil, respectively; P_{ue1}, P_{ue2} and P_{ue3} refer to the winding power loss, core non-load loss and magnetic flux leakage loss, as well as the eddy-current loss of the magnetic leakage in winding, core, outer structure and tank. When t=0, ΔT=0 the steady-state temperature rises of the winding, the core and the transformer oil can be expressed as follows [6]:

$$\Delta T_{u1} = \Delta T_1 - a_{11}e^{\frac{1}{k_1}} - a_{12}e^{\frac{1}{k_2}} - a_{13}e^{\frac{1}{k_3}} \quad (5)$$

$$\Delta T_{u2} = \Delta T_2 - a_{21}e^{\frac{1}{k_1}} - a_{22}e^{\frac{1}{k_2}} - a_{23}e^{\frac{1}{k_3}} \quad (6)$$

$$\Delta T_{u3} = \Delta T_3 - a_{31}e^{\frac{1}{k_1}} - a_{32}e^{\frac{1}{k_2}} - a_{33}e^{\frac{1}{k_3}} \quad (7)$$

α_{ij} is the temperature rise coefficient.

According to formulas (5), (6) and (7), in combination with the transformer parameters, the normal temperature rise and fall curve of the winding, core and transformer oil can be obtained, as shown in Fig. 4. In the initial phase, the winding temperature shows the most obvious trend.

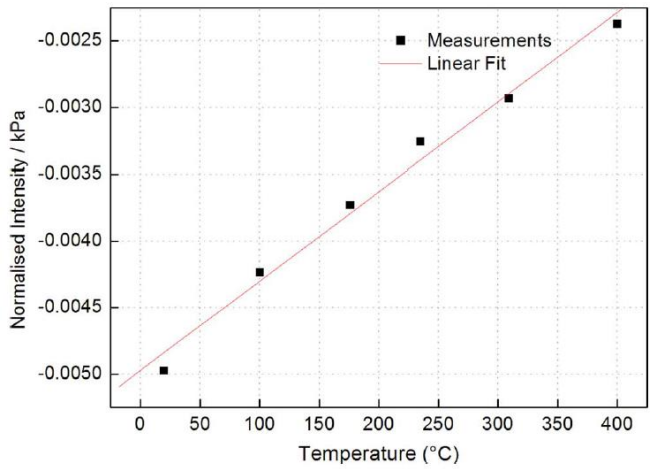

Figure 4. Diagram of the fibre Bragg grating temperature measurement system

Based on the ambient temperature and the running load and considering the correction factor of the viscosity and the temperature loss calculation, this paper establishes an improved model for the transformer winding hotspot temperature (model 3). The model parameters are estimated using the Levenberg-Marquardt method, in the cases of underload (90%), rated load (100%) and overload (110%), respectively. The estimated results and the measured results under different loads are shown in Fig.4, 5. The results show that model 3 can be used to calculate the hotspot temperature of the winding, and has the best calculation accuracy.

In the 90% load case, the hotspot temperature of the transformer winding predicted by model 3 is more accurate than those by model 2 and model 1, showing that taking the correction factor of oil viscosity and the loss calculation of hotspot temperature has a positive impact. This is because the oil viscosity changes with the temperature. The nonlinear thermal resistance, heat capacity and thermal time constants are closely related. With the rated top oil temperature known, the oil viscosity is very essential to the prediction of the hotspot temperature.

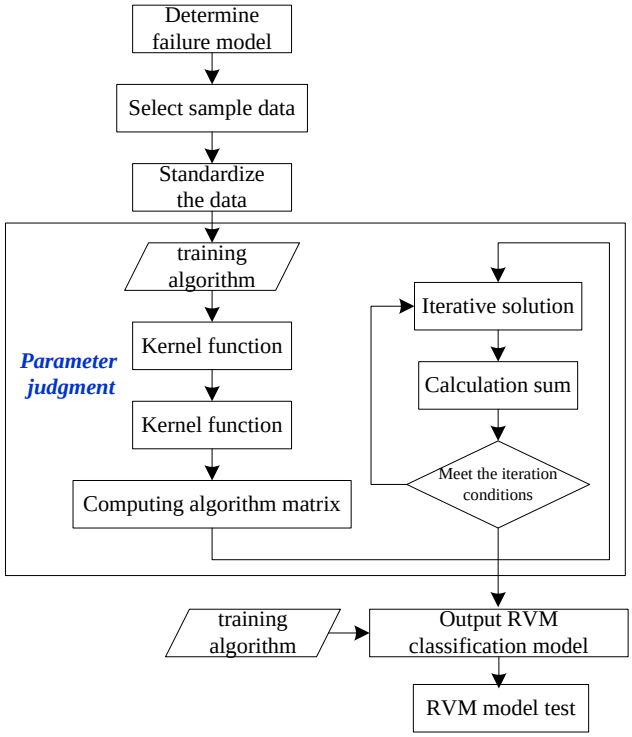

Figure 5. Integrated evaluation model for power transformer fault

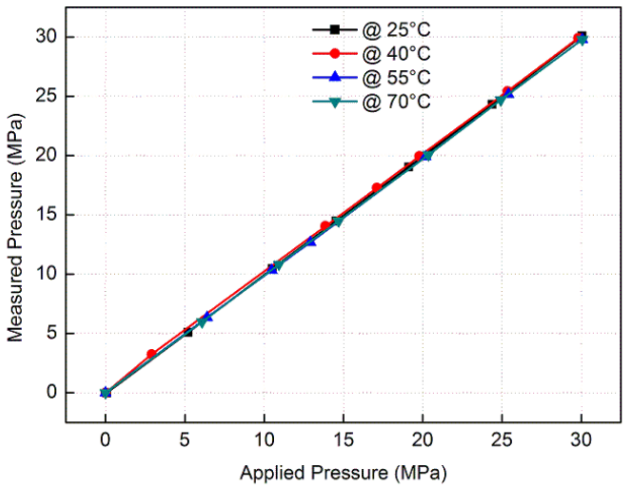

Figure 6. Temperature measurements in 4 stages

The 2 output ends of the optical fibre coupler in the measurement platform are connected with a temperature measurement channel and a wavelength reference channel, respectively. The wavelength reference channel is connected with a reference optical fibre grating and is placed in a constant temperature environment. The temperature measurement channel is connected with the optical fibre grating and is put into the environment where the temperature is to be measured. The relative position of the wavelength peak of each fibre grating can be obtained through photoelectric conversion. Fig.6 shows data acquisition and optical signal processing. Through the collection of the optical fibre grating signal waveforms at different temperatures, the relative positions of wavelength at different temperatures are obtained. The

changes in the peak position of the wavelength of the fibre grating can reflect the changes in temperature [7], [15].

4.2 Repeatability test

Testing conditions, equipment, apparatuses and testing points are identical to those used in the basic error test. At least 3 values are read at every testing point along the same route (in the normal or reverse direction). The maximum difference between the values at every testing point along the same route is the repeatability of the temperature sensor.

A group of testing result curves of the FBG2 temperature sensor are shown in Fig.7. These graphs show that, there is little difference in the three readings of the sensor. The testing procedures for FBG3, FBG4 and FBG5 are identical to those for FBG2, and the repeatability test is conducted on all four measuring gratings, respectively. In the testing results obtained, the maximum difference in the readings is about 1℃.

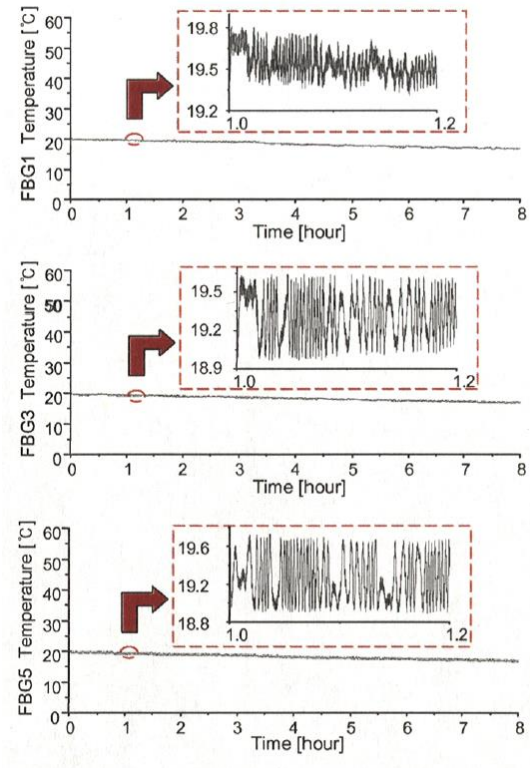

Figure 7. Comparison of the test results of the fibre Bragg grating temperature sensor

In order to verify the effectiveness of the transformer winding hotspot temperature model in different cooling forms and understand the temperature distribution in the oil region, the laboratory built an 100kVA/5kV testing platform to test the transformer model under constant and dynamic loads. Through the adjustment of the short circuit current, various kinds of loads were simulated, and the winding hotspot temperature was calculated based on the temperature rise parameters of the transformer and the parameters estimated by the RVM algorithm. Based on the measured data of the fibre Bragg grating sensors and thermocouples on the temperature rise testing platform, the improved model proved to be effective. Finally, the model was applied in the actual operation of a large oil immersed power transformer, which proves the applicability of the model in the calculation of the transformer winding hotspot temperature.

5. TEST METHOD AND PROCEDURES

The experimental devices are connected according to the optical path above. The FBG sensor is placed in a thermostatic bath. The light signal is sent by the ASE wide-band light source and to the Bragg gratings through a coupler. FBG sends the light spectrum meeting the reflection condition back to the coupler, which will then enters the wavelength demodulation module for analysis and processing to produce relevant parameters In Fig.8, 9, the wavelength demodulation module transmits the processed data to the computer via a serial port. The LabVIEW program calls the synamic link library function to obtain data. The centre wavelength of the reflected light varies with the change of temperature in the thermostatic bath. In this way, a group of 2D data of wavelength signals are obtained. By mapping the wavelength data with the temperature data, we have the final temperature-wavelength curve of the sensor. The measured temperature is obtained real-time by analysis on change of centre wavelength [8]. The collected experimental data of the temperature and the corresponding centre wavelength are shown in the table below:

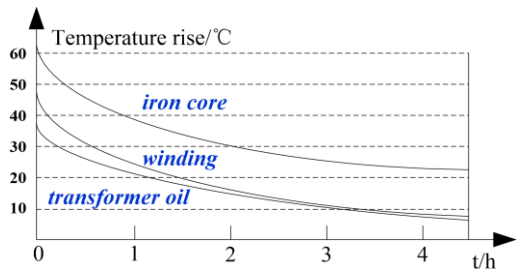

Figure 8. Temperature rise curves of the 3 main transformer components

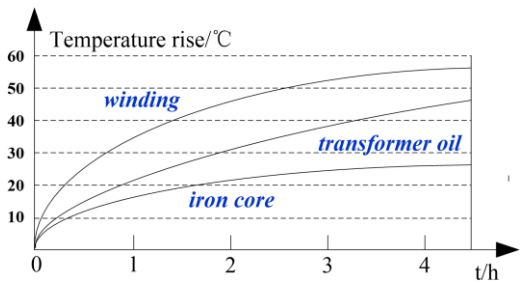

Figure 9. Temperature drop curves of the 3 main transformer components

Table 2. Wavelength/temperature experimental data sheet

Temperature/ ℃	WLT1/nm	WLT2/nm	WLT3/nm	WLT4/nm
30	1520.225	1530.235	1540.425	1550.622
40	1520.343	1530.325	1540.512	1550.702
50	1520.453	1530.415	1540.622	1550.814
60	1520.564	1530.525	1540.723	1550.922
70	1522.085	1531.122	1541.067	1552.023
80	1522.162	1531.235	1541.152	1552.135
90	1522.253	1531.332	1541.245	1552.223

Considering the load of the transformer in operation is periodically dynamically oscillating, it is essential to test the prediction accuracy of the transformer winding hotspot temperature model under dynamic loads. The dynamic load schemes for a transformer include cold start, reduced load and final load removal to verify the dynamic adaptability of the

model. In the low load stage, as shown in Fig.10, the load coefficient is 0.65. As the transformer is no longer in the cold start state, the oil is circulated faster and has higher temperature and lower viscosity than in the previous stage, so the transformer oil temperature will decline rapidly, and accelerate the heat dissipation balance process of the transformer winding.

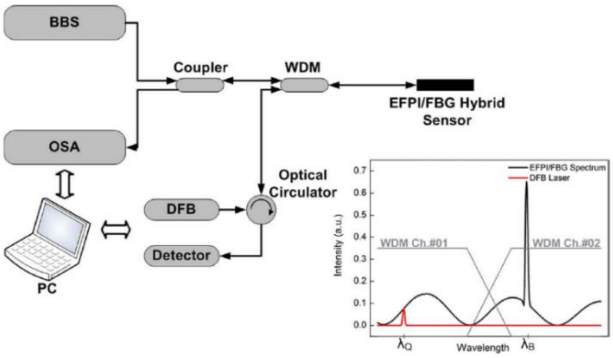

Figure 10. Optical path system and wavelength-related parameters

Once the cooling is down to 37% or so, the oil speed will be much lower than the load reduction speed, and the winding hotspot temperature also decreases slowly. When the load factor is 1.35, the winding hotspot temperature has a short time constant, which makes the hotspot temperature rise rapidly. When the load is removed, due to the short duration of the previous phase, the oil flow is still too late to fully develop, so it is prone to overshoot.

6. CONCLUSION

According to the mathematical model of the sensor, it can be seen that the Bragg wavelength drift of the fibre grating temperature sensor is linear with the change of temperature. Due to the use of different fibre materials and grating technologies, the temperature sensitivity of fibre grating may vary. Therefore, the optical fibre grating sensor need to be calibrated to achieve accurate temperature measurement.

Multiple experiments show that, the FBG sensor has more stable, reliable, and accurate performance than the traditional one. With a higher sensitivity and a greater measurement range, the FBG transformer winding temperature sensor can measure corresponding physical quantities and their changes at several locations.

Being small and light, the FBG probe can detect equipment parameters at locations inaccessible by traditional sensors. It is very suitable for online monitoring of the transformer winding temperature and other parameters. As the FBG sensor directly measures the internal temperature of the transformer, a single optical fibre can connect multiple FBGs with different centre wavelengths in series to realize quasi distributed measurement inside the transformer. Therefore, it has a bright application prospect.

REFERENCES

[1] Reffas A, Idir O, Ziani A, Ameur S, Moulai H, Nacer A, Khelfane I, Rebbouh D. (2016). Combined effect of temperature and electrical discharges on the properties of transformer mineral oils. European Journal of Electrical Engineering 18(1-2): 61-77.

[2] Cataliotti A, Cara DD, Tine G. (2012). Power-line communication in medium-voltage system: Simulation model and on field experimental tests. IEEE Transactions on Power Delivery 27(1): 62-69. http://dx.doi.org/10.1109/TPWRD.2011.2171009

[3] Liu BL, Xu XW. (2017). A power system active power network loss based calculation method on partial priority clustering algorithm. Review of Computer Engineering Studie 4(1): 17-21. http://dx.doi.org/10.18280/rces.040104

[4] Wang FH, Zhou X, Gao P, Xi X. (2015). Improved thermal circuit model of hot spot temperature in oil-immersed transformers based on heat distribution of winding. High Voltage Engineering 41: 895-901. http://dx.doi.org/10.13336/j.1003-6520.hve.2015.03.026

[5] Zhong YC, Wan NF, Xia Y. (2014). Distributed diagnosis algorithm for transformer fault by dissolved gas-in-oil parameters analysis. High Voltage Engineering: 2279-2284. http://dx.doi.org/10.13336/j.1003-6520.hve.2014.08.004

[6] Jiang TS, Li J, Chen WG, Sun CX, Zhao T. (2009). Thermal model for hot spot temperature calculation in oil-immersed transformers. High Voltage Engineering 35(7): 1635-1640.

[7] Gaouda AM, Salama MMA. (2011). DSP wavelet-based tool for monitoring transformer inrush currents and internal faults. IEEE Transactions on Power Delivery 25(3): 1258-1267. http://dx.doi.org/10.1109/TPWRD.2010.2046653

[8] Saleh SA, Rahman MA. (2011). Testing of a wavelet-packet-transform-based differential protection for resistance-grounded three-phase transformers. IEEE Transactions on Industry Applications 46(3): 1109-1117. http://dx.doi.org/10.1109/IAS.2005.1518437

[9] Rao MS, Reddy BE. (2011). Comparative analysis of pattern recognition methods: An overview. Indian Journal of Computer Science & Engineering 2(3): 385-390.

[10] Zhou HQ. (2009). Calculation and design of temperature rise of upper end line section in large transformer winding. Transformer 4: 5-8.

[11] Cao S, Li N, Yu N. (2018). Power electronic transformer control technology based on dsp. Chemical Engineering Transactions 66: 1261-1266. http://dx.doi.org/10.3303/CET1866211

[12] Li JB, Li WH. (1996). Energy method for calculating transformer impedance voltage. Transformer 9: 13-16.

[13] Susa D, Lehtonen M, Nordman H. (2005). Dynamic thermal modelling of ower transformers. IEEE Transactions on Power Delivery 20(1): 197-204. http://dx.doi.org/10.1109/TPWRD.2004.835255

[14] Fan Q. (2018). Multi-target location of infrared image of power equipment. Chemical Engineering Transactions 66: 859-864. http://dx.doi.org/10.3303/CET1866144

[15] Li WP, Zhang ZG. (2009). Analysis on the field of 800kV converter transformer used in HVDC transmission system. Transformer 6: 1-5.